ADVANCED FUNCTIONAL MATERIALS

Supporting Information

for *Adv. Funct. Mater.,* DOI: 10.1002/adfm.201808270

High-T_C Interfacial Ferromagnetism in $SrMnO_3$/$LaMnO_3$ Superlattices

*Marius Keunecke, Fryderyk Lyzwa, Danny Schwarzbach, Vladimir Roddatis, Nicolas Gauquelin, Knut Müller-Caspary, Johann Verbeeck, Sara J. Callori, Frank Klose, Markus Jungbauer, and Vasily Moshnyaga**

High-T_C Interfacial Ferromagnetism in $SrMnO_3/LaMnO_3$ Superlattices

(Supporting Information)

M. Keunecke[1], F. Lyzwa[1,2], D. Schwarzbach[1,3], V. Roddatis[3], N. Gauquelin[4], K. Mueller-Caspary[4,a], J. Verbeeck[4], S. J. Callori[5,6], F. Klose[5,7], M. Jungbauer[1], and V. Moshnyaga[1]

[1]*Erstes Physikalisches Institut, Georg-August-Universität-Göttingen, Friedrich-Hund-Platz 1, 37077 Göttingen, Germany*

[2]Université de Fribourg, Département de Physique, Chemin du Musée 3, 1700 Fribourg, Switzerland

[3]*Institut für Materialphysik, Georg-August-Universität-Göttingen, Friedrich-Hund-Platz 1, 37077 Göttingen, Germany*

[4]*EMAT, University of Antwerp, Groenenborgerlaan 171, 2020 Antwerp, Belgium*

[5]*Australian Centre for Neutron Scattering, ANSTO, New Illawarra Road, Lucas Heights, NSW 2234, Australia*

[6]*Department of Physics, California State University, San Bernardino, California 92407, USA*

[7]*Guangdong Technion-Israel Institute of Technology 241, Da Xue Road Shantou, 515063, PR China*

[a] *present address: Forschungszentrum Jülich; Physics of Nanoscale Systems (ER-C-1), Wilhelm-Johnen-Straße, 52425 Jülich, Germany*

S1. Surface morphology studied by scanning tunneling microscopy (STM).

Examples of the STM surface morphology of the SL with n=3 grown on STO(100) and LSAT substrates are shown in Fig. S1. One can see typical features of a step-flow growth with one-atomic height terraces of the width, W~100-200 nm, originating from a miscut of substrates. The values of surface mean-square STM roughness, RMS=0.2-0.3 nm, measured for different SLs agree well with XRR simulations (see Fig. S2). Moreover, at the surface of SLs, terminated with LMO layer (the starting layer was SMO), we observed wave-like vertical corrugations with a height of ~0.02 nm and the wavelength ~30 nm, spreading across the terrace edges. We believe their presence reflects a long-range strain relaxation at the surface due to the cooperative Jahn-Teller (JT) distortion in the topmost LMO layer.

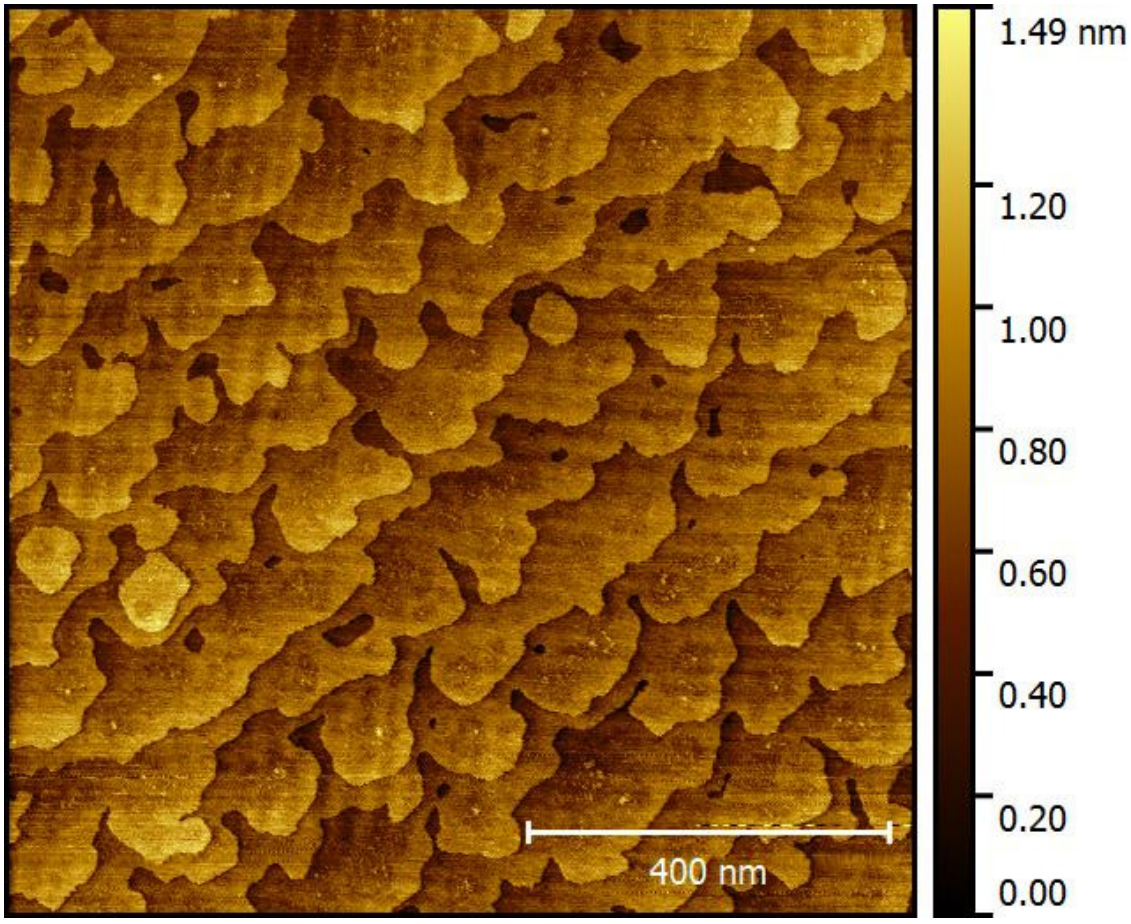

Fig. S1 STM surface morphology of an SL with n=3, grown on $SrTiO_3$(001) substrate.

S2. X-ray diffraction and X-ray reflectometry (XRR) of SLs with n=1-5.

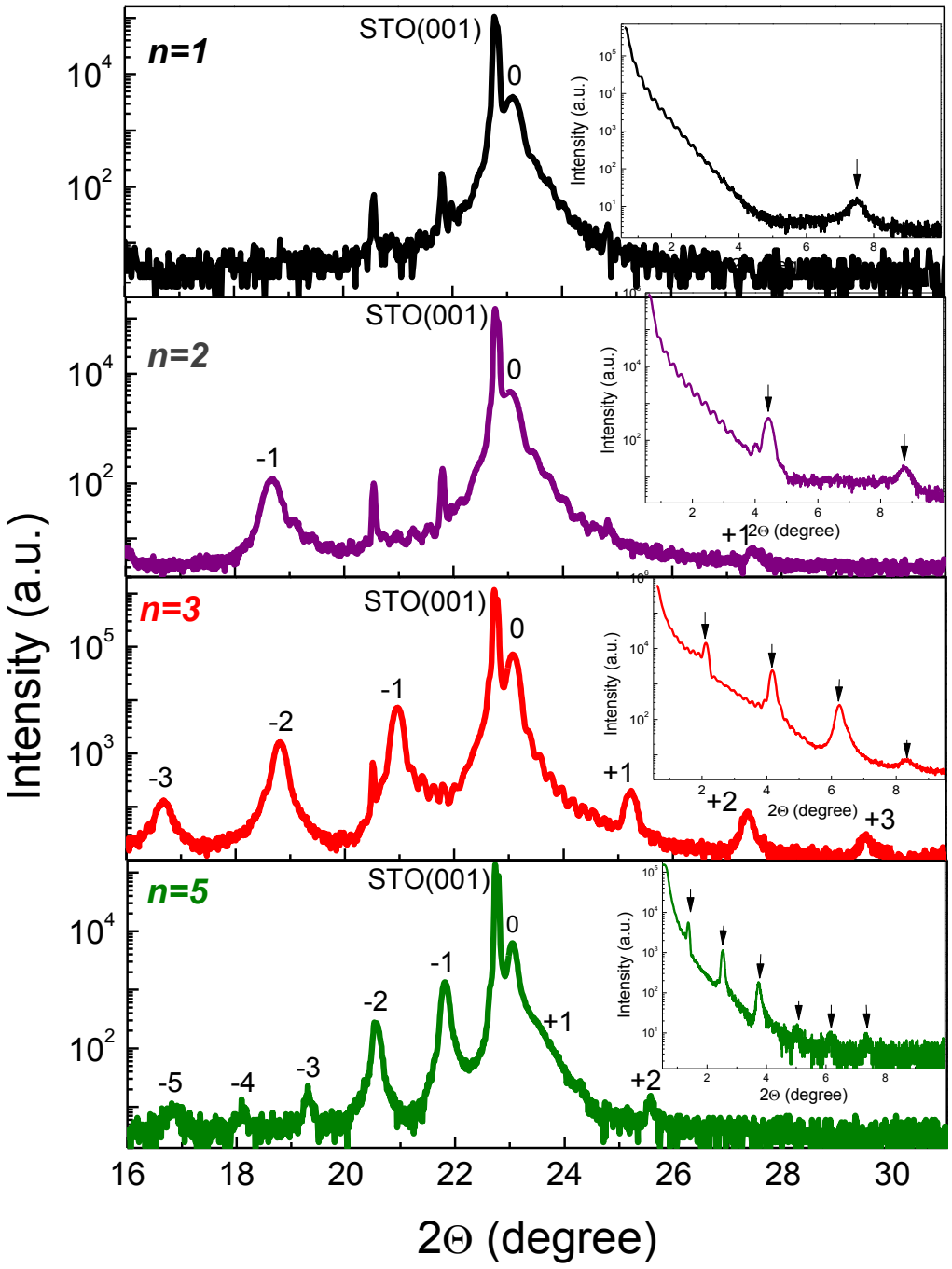

Fig. S2 X-ray diffraction patterns around the substrate STO(001) peak and small-angle X-ray reflectivity (insets) of SLs with n=1-5, grown on STO(001) substrates.

S3. Simulations of small-angle X-ray reflectometry (XRR).

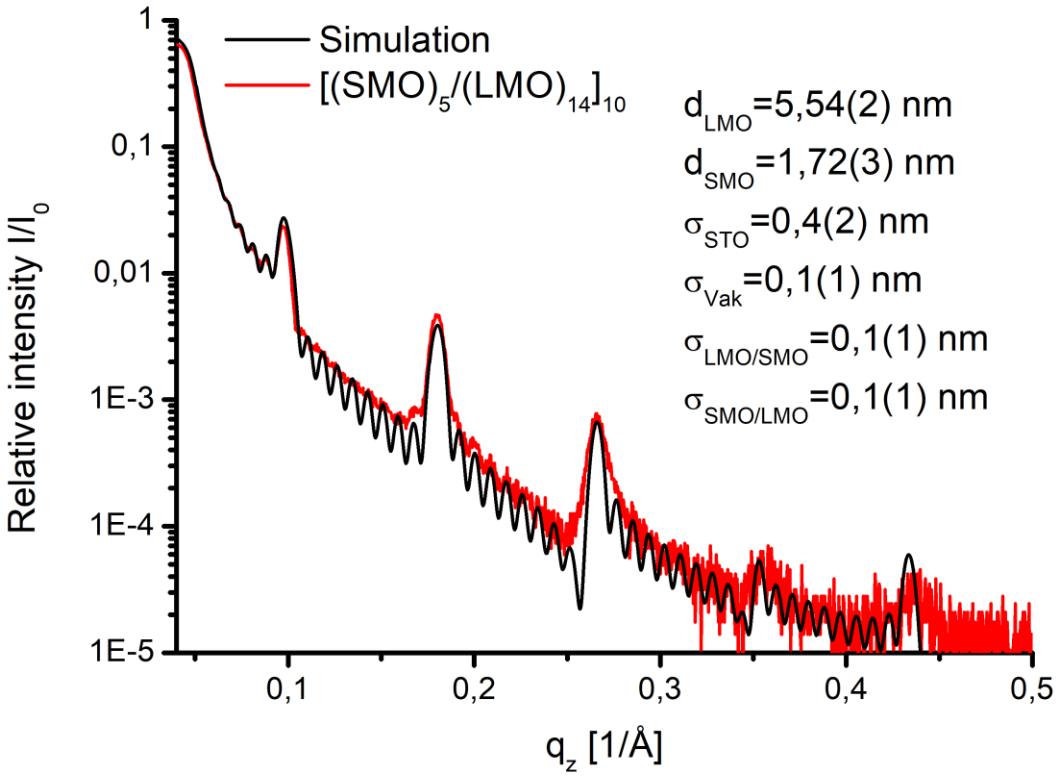

Fig. S3 The measured (red) and simulated (black) XRR curve of the SL with n=5. Simulations were performed by means of the program ReMagX [30], which uses the Paratt algorithm to calculate the XRR spectra of the superlattices. We set the thicknesses of LMO (d_{LMO}) and SMO (d_{SMO}) layers as well as the mean-square roughness ($\sigma_{SMO/LMO}$ & $\sigma_{LMO/SMO}$) to be the same for every bilayer in the SL to simplify simulations. The roughness of the uppermost layer (LMO) was simulated separately (σ_{vac}).

S4. Simulations of X-ray diffraction (XRD) in the Bragg-Brentano geometry.

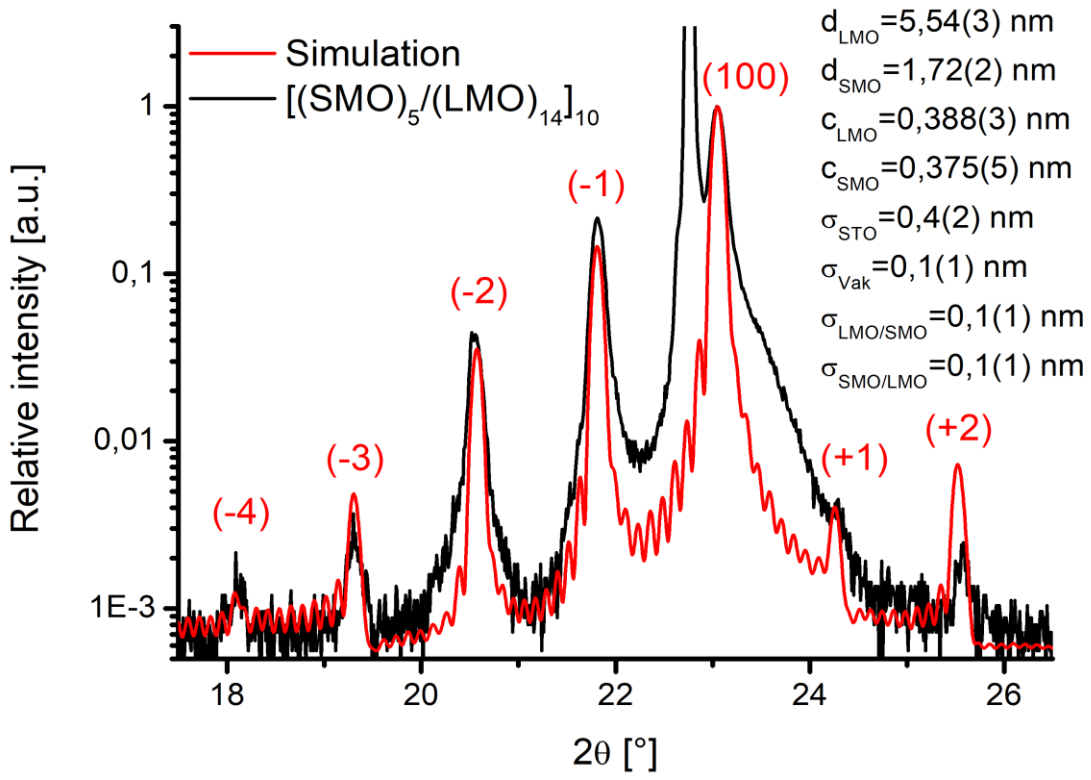

Fig. S4 The measured (black) and simulated (red) θ-2θ XRD pattern of the SL with n=5. Simulations were carried out by means of the program "XrayWW" [44], which artificially separates the SL into N layers with corresponding thickness d_i, chemical composition at the A-place (A_i) and B place (B_i), roughness σ_i and lattice parameter c_i. The intensity ratios of the satellite peaks are determined by calculating the structural factor, corrected for the dependence of scattering vector on the atomic form factors and the crystallographic Lorentz factor.

S5. Electrical resistivity of SLs (n=1-5) compared to that of single LSMO and LMO films.

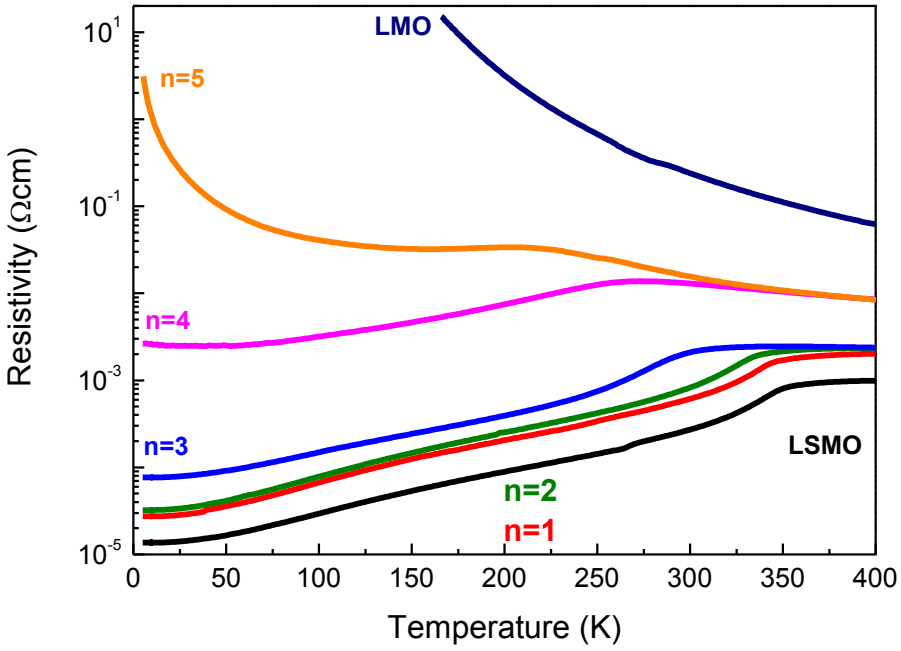

Fig. S5 Resistivity vs temperature of SLs and thin LSMO/STO and LMO/STO films (d=40 nm).

S6. Details of local structure: HAADF intensity profile and EELS fine structures

The abruptness of the interfaces was analysed by Z-contrast STEM, which is especially sensitive to the chemical composition at the A-sites of the perovskite lattice. In particular, we defined two basis vectors (see the inset of Fig. S6) and used them to detect all atomic columns in the underlying annular dark field Z-contrast image. The atomic column positions have then been refined to subpixel accuracy by fitting Gaussians to the local intensity maxima. In order to calculate the integral intensity of each atomic column, a "Voronoi diagram" (see Ref. 35) was calculated as shown exemplarily in red for one Voronoi-cell of the A-sublattice in the inset. On the right hand side, the Voronoi intensities of the A-sites are mapped colour-coded, together with their profile along the growth direction, revealing chemically sharper SMO/LMO interface compared to the LMO/SMO interface. Note, that the length scale of th "less sharp" LMO/SMO and "sharp" SMO/LMO interfaces is limited to 1-2 u.c. and less than 1 u.c., respectively.

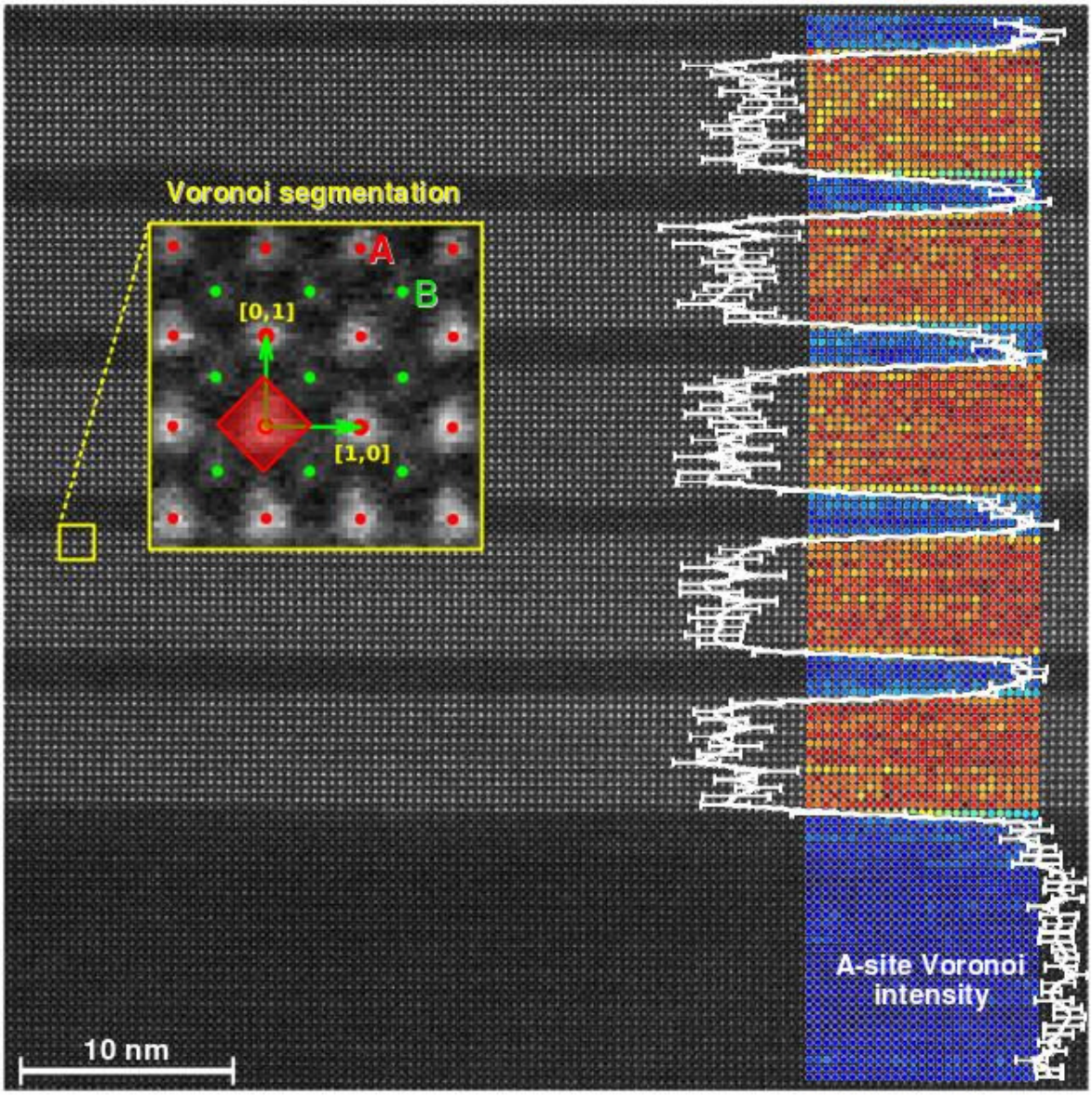

Fig. S6: HAADF-STEM image of the SMO/LMO superlattice with the A-site “Voronoi intensity” represented as a color code for each unit cell on the right hand of the figure, the resulting intensity profile is overlayed as a white line on top of the STEM image.

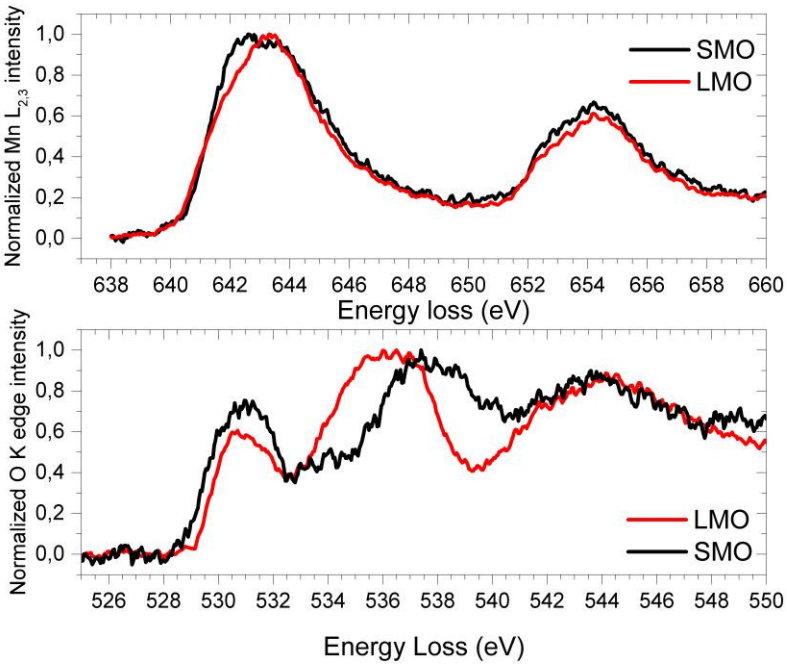

Fig. S7 The Mn L2,3 edge fine structure of the LMO and SMO layers (top panel) shows the presence of some Mn^{4+} ions in the SMO. The O K edge fine structure (bottom) in the LMO and SMO layers demonstrates a strong difference between the bonding of oxygen in these two layers. The spectra are similar to the reference spectra of the SMO and LMO (see Ref. 35).

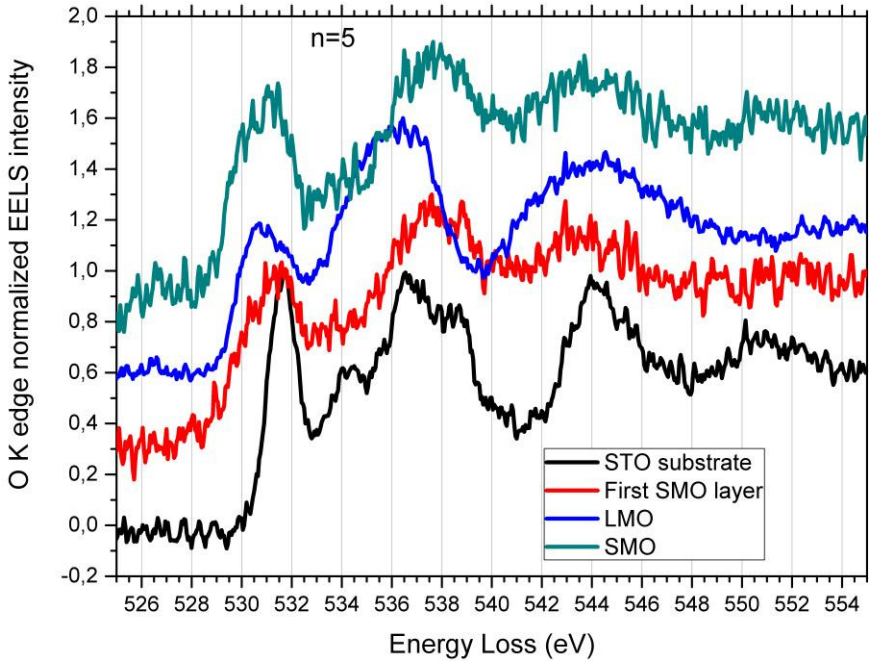

Fig. S8: Fine structures of the O K edge in the first SMO layer, compared to the subsequent layers of LMO and SMO as well as of the STO substrate. This shows that the electronic structure in the first SMO layer is identical to that of each subsequent SMO layers, proving the absence of interdiffusion in the specimen.

S7. Magnetic behavior of SLs with different thicknesses of SMO and LMO compared to the LSMO film (n=0).

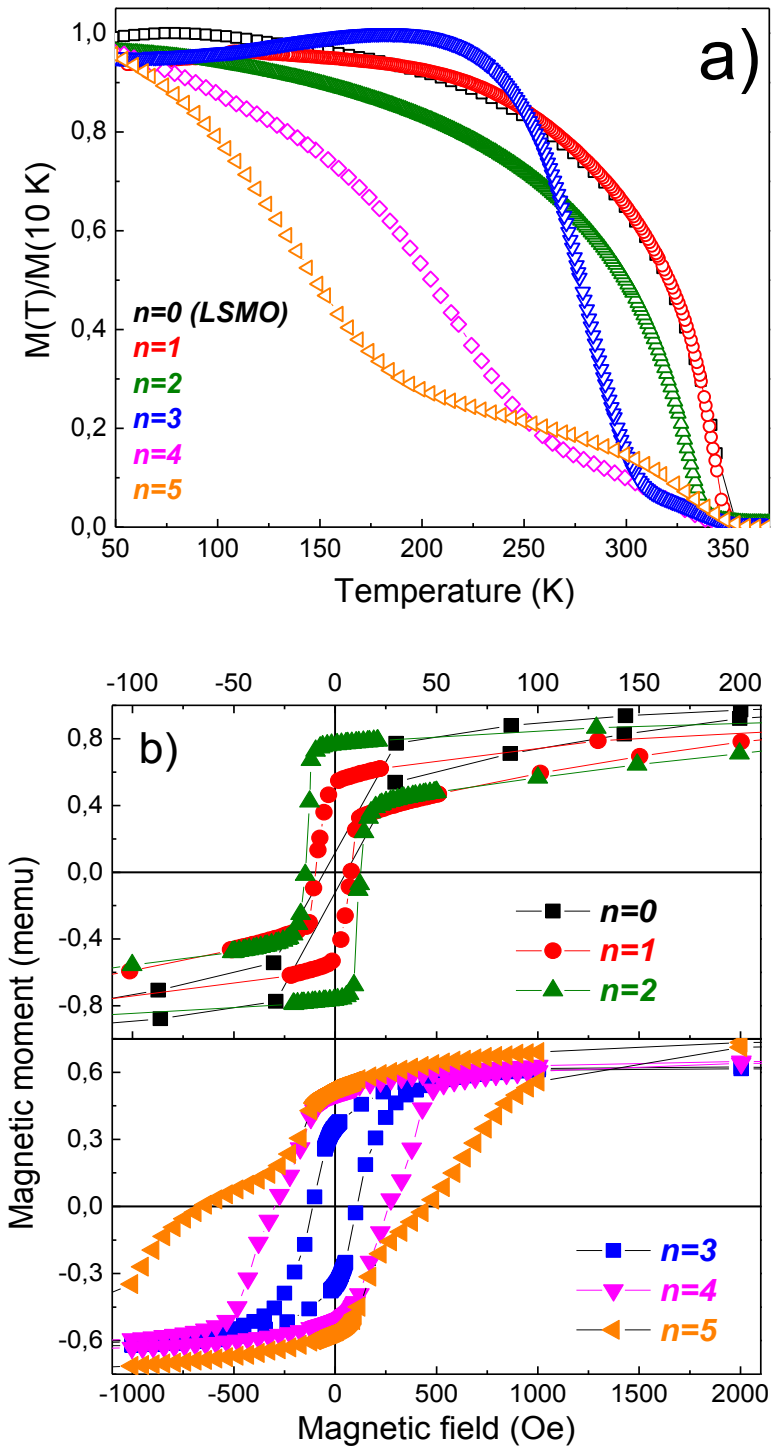

Fig. S9: a) Temperature dependences of the normalized magnetic moment, M(T)/M(10K), of LSMO (n=0) and SLs with n=1-5; b) M(H) field dependences at T=10 K for LSMO and SL's display low coercive field and homogeneous LSMO-like behavior for SL's with n=1, 2 and an FM/AFM coexistence for n=3-5;

S8. Ellipsometry model.

The in situ measured ellipsometry signal (see Fig. 6) was simulated by using a simple optical model, based on the Fresnel coefficients and Snell's law (see also Ref. 44). The thickness of the SMO and LMO single perovskite unit cells were taken from the XRD data and simulations, i.e. D_{SMO}=0.375 nm and D_{LMO}=0.388 nm and the angle of incidence of φ=62.05. To obtain the "blue" curve in Fig. 6, which reproduces the optical behavior in the (SMO_5/LMO_{14}) without charge transfer, the complex refractive indices, i.e. n_{SMO}=2.71+i*0.95 and n_{LMO}=2.4+i*0.45 were obtained from the ellipsometry measurements on single LMO and SMO films with thickness, D=40 nm, grown on STO substrates at a deposition temperature of T=900°C (Ref. 45). To get the theoretical "green" curve in Fig. 6 we simulated the electron transfer by modifying the refractive index within first 2 u.c. in each SMO layer by replacing them with artificial electron-rich layers, having optical parameters of $La_{1-x}Sr_xMnO_3$ (x=0-1) as shown in Tab. S1.

Tab. S1. Fit parameters used for the optical model for the curve with (blue colour) and without (green colour) charge-transfer (CT) at the SMO/LMO interface. We used an angle of incidence of φ=62.05 and refractive indices of n_{STO}=2.34 (substrate) and n_{air}=1.00027 (ambient air).

<table>
<tr><th></th><th>Without CT</th><th colspan="3">With CT</th></tr>
<tr><td>$(LaMnO_3)_{14}$ -layer</td><td>n_{LMO}=2.4 + 0.45i
d_{LMO}=5.543 nm</td><td colspan="3">n_{LMO}=2.4 + 0.45i
d_{LMO}=5.543 nm</td></tr>
<tr><td rowspan="10">$(SrMnO_3)_{4.8}$ -layer</td><td rowspan="10">n_{SMO}=2.71 + 0.95i
d_{SMO}=1.802 nm</td><td></td><td>Doping level</td><td>Fit parameters</td></tr>
<tr><td rowspan="6">~2 u.c.
(CT occurring)</td><td>x=0.1</td><td>n_1=2.39 + 0.43i
d_1= 0.025 nm</td></tr>
<tr><td>x=0.2</td><td>n_2=2.36 + 0.45i
d_2= 0.025 nm</td></tr>
<tr><td>x=0.3</td><td>n_3=2.25 + 0.55i
d_3=0.49 nm</td></tr>
<tr><td>x=0.4</td><td>n_4=2.46 + 0.54i
d_4=0.06 nm</td></tr>
<tr><td>x=0.5</td><td>n_5=2.6 + 0.65i
d_5=0.06 nm</td></tr>
<tr><td>x=0.6</td><td>n_6=2.74 + 0.85i
d_6=0.06 nm</td></tr>
<tr><td>~1 u.c.
(decrease of dΔ/dD down to SMO level)</td><td>x=0.8</td><td>n_7=2.79 + 0.92i
d_7=0.36nm</td></tr>
<tr><td rowspan="2">~2 u.c.
(usual SMO-layer)</td><td>x=1 (SMO)</td><td>n_8=2.71 + 0.95i
d_{SMO}=0.67 nm</td></tr>
<tr><td>Transition SMO to LMO-layer (reconstructed)</td><td>n_9=2.55 + 0.7i
n_9=0.05 nm</td></tr>
</table>

Such modified SMO layer consists of ~2 u.c. where the charge transfer itself takes place, accompanied with unusual increase and maximum in Δ(D) (Fig. 6). The second part ~1 u.c. is represented by the following decrease of the slope dΔ/dD down to the SMO level. For the remaining 2 u.c. SMO we used the same model parameters as in the simulation without a charge transfer. The refractive indices for those artificial LSMO layers were first taken as in Ref. 44 and then slightly adjusted to better reproduce the data.

References

35. A. Rosenauer, Th. Mehrtens, K. Müller, K. Gries, M. Schowalter, P. V. Satyam, S. Bley, Ch. Tessarek, D. Hommel, K. Sebald, M. Seyfried, J. Gutowski, A. Avramescu, K. Engl, S. Lutgen, *Ultramiscrosopy* **2011**, *111*, 1316.
36. A. Galdi, C. Aruta, P. Orgiani, C. Adamo, V. Bisogni, N.B. Brookes, G. Ghiringhelli, D.G. Schlom, P. Thakur, and L. Maritato *Phys. Rev. B* **2012**, *85*, 125129.
44. F. Lyzwa, P. Marsik, V. Roddatis, C. Bernhard, M. Jungbauer, V. Moshnyaga, J. Phys. D: Appl. Phys. **2018**, *51*, 125306.
45. M. Jungbauer, Gestaltung der elektronischen Korrelationen in Perowskit-Heterostrukturen auf atomarer Skala. *Dissertation Georg-August-Universität Göttingen*, **2016** p. 96.